Rectifying Group Irregularities in Explanations for Distribution Shift

Adam Stein **Yinjun Wu** **Eric Wong** **Mayur Naik**
{STEINAD, WUYINJUN, EXWONG, MHNAIK}@SEAS.UPENN.EDU
University of Pennsylvania

Abstract

It is well-known that real-world changes constituting distribution shift adversely affect model performance. How to characterize those changes in an interpretable manner is poorly understood. Existing techniques take the form of shift explanations that elucidate how samples map from the original distribution toward the shifted one by reducing the disparity between the two distributions. However, these methods can introduce group irregularities, leading to explanations that are less feasible and robust. To address these issues, we propose Group-aware Shift Explanations (GSE), an explanation method that leverages worst-group optimization to rectify group irregularities. We demonstrate that GSE not only maintains group structures, but can improve feasibility and robustness over a variety of domains by up to 20% and 25% respectively.

1 Introduction

Classic machine learning theory assumes that training and testing data are sampled from the same distribution [1]. Unfortunately, distribution shifts infringe on this requirement and can drastically change a model's behavior [2]. For instance, training a model on data collected from one hospital may result in inaccurate diagnoses for patients from other hospitals due to variations in medical equipment [3]. Similarly, shifts from day to night or from clear to rainy weather are obstacles for autonomous driving [4].

When such a distribution shift occurs, it is often useful to understand *why* and *how* the data changed, independent of the model [5]. For example, suppose a doctor observes their medical AI model's performance degrading. Before modifying the model, the doctor should first understand how their patient data changed [6]. Similarly, a self-driving engineer would have an easier time adapting their system to a new environment if it was known that the shift resulted from changing weather conditions [7].

The predominant method to understand a distribution shift is a *shift explanation* [8]. A shift explanation maps the original distribution (the source) to the shifted one (the target) to reduce their disparity. For example, Kulinski and Inouye [8] find a direct mapping of points from the source toward the target via optimal transport [9] and its variant, K-cluster transport. Another approach is to use counterfactual explanation methods such as DiCE [10] to explain a classifier between the source and target distributions.

State-of-the-art shift explanations seek to optimize global objectives, e.g. minimizing the difference between the target and the mapped source distribution [8]. However, these optimal mappings are not necessarily good explanations: they may be infeasible or lack robustness to source perturbations.

As an example, Figure 1 shows explanations from existing work that we learned to map individuals with low income (source distribution) to individuals with high income (target distribution) in the

XAI in Action: Past, Present, and Future Applications @ NeurIPS 2023.

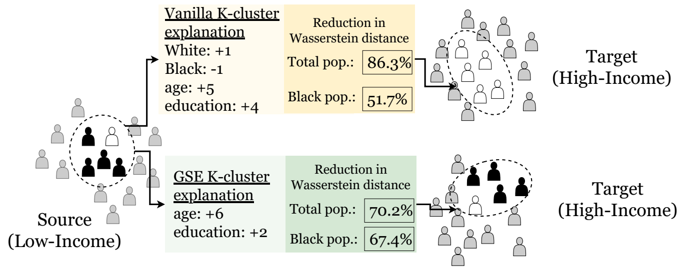

(a) Cluster level shift explanation.

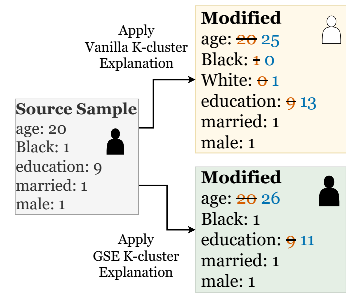

(b) Instance level shift explanation.

Figure 1: (a) Compares shift explanations we learned from low to high-income populations using Vanilla and GSE K-cluster transport methods on the Adult dataset. Vanilla alters the race of a predominantly Black subpopulation, while GSE maintains Black and White subpopulations by slightly adjusting age (+6 years) and maximum education level (+2 years). (b) Illustrates instance-level explanations we learned; Vanilla changes race while our method does not. Full results in Appendix F.1.

Adult dataset [11]. Such explanations can help reveal insights about income inequalities that enable a policymaker to propose better policies or an individual to understand how to increase their income. At a dataset level, we see in Figure 1a that K-cluster transport can produce a shift explanation that effectively maps the source distribution to the target, resulting in an 86.3% reduction in the Wasserstein distance between these two distributions. However, upon closer inspection, this explanation shifts a majority Black cluster to a majority White cluster. Focusing on the Black racial subpopulation of the source and target, the explanation only decreases the Wasserstein distance by 51.7%. Such an explanation is not useful if such changes to race are considered infeasible[1].

Our key insight to achieving high-quality shift explanations is to steer the generated explanations to respect subpopulations, or **groups**, in the data. Since groups are highly context-specific, we seek an approach that is general and still produces overall good explanations. In our running example, assuming race-based grouping, such an approach should yield a mapping that minimizes disruptions to the groups while maximizing overall fitness. As depicted at the bottom of Figure 1a, we achieve such a mapping using the *same* underlying K-cluster transport method, that increases the reduction of Wasserstein distance between source and target samples from 51.7% to 67.4% within the Black subpopulation, and has a small impact on the reduction of Wasserstein distance between the overall source and target populations (from 86.3% to 70.2%).

To this end, we propose Group-aware Shift Explanations (GSE), an explanation method for distribution shift that preserves groups (equivalently conditional densities) in the data. We develop a unifying framework that allows us to apply GSE to heterogeneous methods for producing shift explanations including both optimal transport and counterfactual explanation methods, making them maintain group structures and enhancing their feasibility and robustness. Through extensive experiments over a wide range of tabular, language, and image datasets, we demonstrate that GSE not only maps source samples closer to target samples belonging to the same group, thus preserving group structure, but also boosts the feasibility and robustness by up to 23% and 42% respectively.

Our main contributions are summarized as follows:

1. We identify group irregularities as a class of problems that can adversely affect the quality of shift explanations, and we validate their existence empirically and theoretically.
2. We propose Group-aware Shift Explanations (GSE) to rectify group irregularities when explaining distribution shift, and enhance the feasibility and robustness of the shift explanations simultaneously, which are justified theoretically.
3. We propose a general framework to unify heterogeneous shift explanation methods, allowing the use of GSE for a wide range of shift explanation methods and domains.

[1] We note that the race attribute is not generally infeasible and decisions of infeasibility are left to the user.

4. We empirically demonstrate over a diverse set of datasets how GSE maintains group structures and enables more feasible and robust shift explanations.

2 Motivation

Distribution shift is any change from an initial (source) to a different (target) distribution. We follow Kulinski and Inouye [8] to define a shift explanation as a mapping from the source to the target distribution. For instance, Figure 1 shows a K-cluster explanation from our experiments which maps the source to the target distribution by changing race among other changes. In this section, we empirically identify issues with all existing shift explanations in terms of group irregularities.

To find a shift explanation, state-of-the-art methods primarily minimize the disparity between the source and the target distribution. For example, K-cluster transport minimizes an objective depending on the Wasserstein distance between the source and the target distribution. However, this is not sufficient for finding high-quality explanations. Figure 1 shows such an example with K-cluster explanations where a majority Black subpopulation of the source gets mapped to a majority White subpopulation of the target. In this case, the overall Wasserstein distance is reduced by 86.3%, but the Wasserstein distance for the Black subpopulation is reduced much less in Figure 1a. Our full results in Table 1 show that this problem is pervasive across the datasets and shift explanations we considered.

Impact on Explanation Feasibility Shift explanations which break apart groups of the data can also be overall *infeasible*. Feasibility is a measure of how useful an explanation is to a downstream user, quantified by the percent of the source samples it is useful for. For instance, in Figure 1, the race attribute may be less actionable than others, so a K-cluster explanation which modifies the race attribute would be useless for a policymaker who designs policies to help increase the income of the low-income population. Overall, the K-cluster explanation from our experiments shown in Figure 1 is only feasible for 21.0% of the source distribution, meaning that 79.0% of the source samples have their race changed by the shift explanation. Later, we show how our method, which rectifies these group irregularities, results in more feasible explanations for the overall source distributions.

Impact on Explanation Robustness Group irregularities can also reduce *robustness*, meaning that small changes to a source distribution result in large changes to the shift explanation. Figure 2 shows an example of poor explanation robustness from our experiments on the Adult and Civil Comments datasets. In Figure 2a, a small perturbation to the source distribution leads to the explanation modifying the race feature for a cluster of the data. Figure 2b shows a shift explanation that maps a non-toxic sample relating to medicine into the target distribution of toxic sentences. After a small perturbation, the explanation maps the same sample by adding the words "shooter" and "stupid" which is an unfeasible change since it changes the topic of the sample to violence. Ideally, we want a shift explanation to be robust to very small changes to the source distribution since it should explain general behavior instead of relying on minute details of a distribution.

Lastly, to formally validate that group irregularities are a fundamental problem, we study a simple 1D setting in Section 3.4 where we show that group irregularities always exist for explanations that optimize the reduction in Wasserstein distance between the source and target.

3 Group-aware Shift Explanations (GSE)

In this section, we discuss our method applied to K-cluster explanations and formalize the notions of feasibility and robustness introduced in Section 2 as metrics for evaluating shift explanations. We give details in Appendix A for how to generalize our method to support most shift explanation methods and diverse datasets including text and image data.

3.1 Preliminaries on K-cluster transport and PercentExplained (PE)

The shift explanations produced by K-cluster transport can be denoted by a mapping function $M(x;\theta_x)$ which maps a source sample x towards the target distribution by a learnable distance

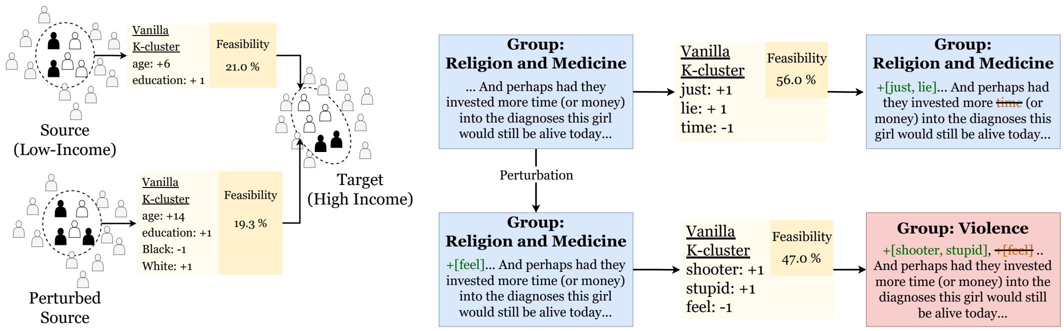

(a) Adult dataset. (b) Civil Comments dataset.

Figure 2: Poor explanation robustness illustrated. Even if an explanation is feasible for a subpopulation (top), small perturbations to the source distribution can make it become infeasible (bottom). (b) Illustration of explanation robustness issues in the Civil Comments dataset, shifting from non-toxic to toxic text using KMeans-defined groups. More details on the group derivation are in Appendix E.

of θ_x. As the name K-cluster transport suggests, all the source samples are grouped into a set of clusters, C, with K-means clustering, and all the samples within one cluster, $c \in C$, share the same θ_c. Therefore, the mapping function for K-cluster transport is formulated as follows:

$$M(x;\theta) = x + \sum\nolimits_{c \in C} \mathbf{1}_{x \in c} \theta_c, \text{ in which, } \theta = \{\theta_c | c \in C\}.$$

Optimizing θ. According to Kulinski and Inouye [8], θ is solved by maximizing PercentExplained (PE). Suppose the source distribution and the target distribution are denoted by P and Q respectively, then PE is formulated as the following:

$$\text{PE}(\theta; M, P, Q) = 1 - W_2^2(M(P;\theta), Q)/W_2^2(P, Q), \tag{1}$$

where $W_2(\cdot)$ is the Wasserstein-2 distance and $M(P;\theta)$ is notation for the mapping M applied to every sample in the source, i.e. $M(P;\theta) = \{M(x;\theta) \mid x \in P\}$. Intuitively, PE quantifies how much the mapping $M(\cdot;\theta)$ reduces the distance between P and Q. A high PE means that the explanation, $M(\cdot, \theta)$, closely matches the overall source to the overall target distribution. We can directly optimize PE using gradient descent using a differentiable implementation of the Wasserstein-2 distance such as the GeomLoss library's [12].

3.2 Feasibility and Robustness Metrics

We formalize the metrics of feasibility and robustness, as introduced in Section 2.

Feasibility Counterfactual explanation literature has already defined feasibility [13]. Formally, feasibility is the percentage of source samples with feasible explanations, i.e.:

$$\text{\% Feasible} = \left[\sum\nolimits_{x \in P} a(x, M(x;\theta))\right] / \|P\| \tag{2}$$

where $a(\cdot, \cdot)$ is 1 when the change from x to $M(x;\theta)$ is feasible, and 0 otherwise (say changing education is feasible while changing sex is infeasible for the Adult dataset).

Robustness The notion of robustness is also proposed in prior work [14, 15]. We define two robustness metrics (denoted by Ω and Ω_{worst} respectively) which are adapted from the robustness metrics from Alvarez-Melis and Jaakkola [14]:

$$\begin{aligned} &\Omega(\theta; M, P, Q, \epsilon) = \|M(P;\theta) - M(P(\epsilon);\theta(\epsilon))\|_2 / \|P - P(\epsilon)\|_2, \\ &\Omega_{\text{worst}}(\theta; M, P, Q) = \max\nolimits_\epsilon \Omega(\theta; M, P, Q, \epsilon), \end{aligned} \tag{3}$$

in which θ and $\theta(\epsilon)$ are derived by finding a shift explanation with the source distribution as P, or the perturbed source distribution $P(\epsilon)$, respectively. Details on producing a perturbation ϵ and solving for Ω_{worst} are provided in Appendix D.5.

Table 1: Comparison of PE, WG-PE, and %Feasible metrics between vanilla and GSE K-cluster explanations (Higher is better).

	PE ↑		WG-PE ↑		%Feas ↑	
	Vanilla	GSE	Vanilla	GSE	Vanilla	GSE
Breast	**97.56±0.00**	96.89±0.00	83.42±0.00	**93.42±0.00**	34.43±0.00	**35.38±0.00**
Adult	**99.83±0.01**	97.40±0.04	75.13±0.06	**96.16±0.02**	86.63±0.12	**89.27±2.18**
Civil	0.63±0.10	**0.88±0.10**	0.62±0.10	**0.83±0.11**	90.30±0.80	**91.07±0.05**
Amazon	-2.23±0.03	**-1.11±0.66**	-2.41±0.03	**-1.17±0.73**	87.00±0.00	87.00±0.00
ImageNet	18.26±1.75	**20.07±3.45**	-8.61±4.02	**-3.78±7.65**	37.25±4.58	**50.11±4.94**
FMoW	**18.73±0.00**	13.02±0.00	-17.30±0.00	**7.46±0.00**	50.20±0.00	**54.55±0.00**
iWildCam	14.60±1.29	**15.71±0.68**	**2.39±2.07**	-1.32±0.76	48.69±2.28	**71.24±2.05**

Table 2: Comparison of Robustness and Worst-case Robustness between vanilla and GSE K-cluster explanations (Lower is better).

	Method	Adult	Breast	Civil	Amazon	ImageNet	FMoW	iWildCam
Rob. ↓	Vanilla	**1.34±0.28**	6907.79±3577.96	10.10±2.26	18.78±11.06	36.56±10.43	**8.26±0.73**	8.48±1.51
	GSE	1.52±0.40	**6500.83±3270.29**	**10.02±2.19**	**13.95±6.04**	**35.47±11.26**	20.40±4.90	**8.47±1.14**
WC Rob. ↓	Vanilla	**1.74**	16086.54	16.59	38.14	59.19	**9.62**	11.94
	GSE	2.18	**15438.47**	**15.32**	**26.86**	**56.04**	28.05	**10.34**

3.3 Worst-group PE for GSE

To rectify the issues identified in Section 2 in existing shift explanations, we can ideally optimize PE for all pre-specified groups. This ideal, however, is not applicable to finding dataset-level explanations since it requires an explanation per group, increasing explanation complexity by a factor of the number of groups. Instead, we propose Group-aware Shift Explanations (GSE) to optimize the *worst-group PE*, which leads to implicitly improving PE for *all groups* simultaneously.

Specifically, suppose the source and target are partitioned into G disjoint groups, i.e., $P = \{P_1, P_2, \ldots, P_G\}$ and $Q = \{Q_1, Q_2, \ldots, Q_G\}$, in which, P_g and Q_g belong to the same group, e.g., the male sub-populations from P and Q. We can then evaluate PE on a shared group from the source and target. The worst-group PE is calculated over all G groups as the following:

$$\text{WG-PE}(\theta; M, P, Q) = \min_g \text{PE}(\theta; M, P_g, Q_g). \tag{4}$$

This metric indicates how much the distance between any pair of P_g and Q_g is reduced, in the *worst case*. Optimizing θ to maximize WG-PE can guarantee that for *every* pair of P_g and Q_g, $\text{PE}(\theta; M, P_g, Q_g)$ is not approaching 0.

3.4 Theoretical Analysis

We theoretically analyze the existence of group irregularities in a simple 1D setting and show that our worst-group optimization method mitigates the problem.

Theorem 1. *Suppose $P = \text{Bernoulli}(p)$ and $Q = \alpha \cdot \text{Bernoulli}(p) + \beta$ in one dimensional setting where $p \in [0, 1]$ and $\alpha, \beta \in \mathbb{R}$ such that $\alpha + 2\beta \neq 1$. We further split the joint distribution of P and Q into two groups depending on the sampling results, i.e., Group$(x) = 1$ if $x \sim P$ and $x = 0$ or $x \sim Q$ and $x = \beta$, and Group$(x) = 2$ otherwise. Let $M(x; \theta_{PE}) = x + \theta_{PE}$ and $M(x; \theta_{WG}) = x + \theta_{WG}$ be two K-cluster explanations (K=1) which are solved by maximizing PE(θ) and WG-PE(θ) respectively. Then, PE$(\theta_{WG}) -$ WG-PE$(\theta_{WG}) = 0$ for all α, β, and p while PE$(\theta_{PE}) -$ WG-PE$(\theta_{PE}) > 0$ except when $p = \frac{\beta}{\alpha + 2\beta - 1}$ or $p = \frac{\beta}{1 - \alpha}$ holds.*

The takeaway is that group irregularities, or a disparity between the overall PE and worst-group PE, exist when optimizing the overall PE. We also theoretically analyze the feasibility and robustness of shift explanations in this setting in Appendix J.

4 Experiments

We present our experiments for evaluating the effectiveness of GSE compared to shift explanations which ignore group structures. In what follows, we describe the datasets and experimental setup in Section 4.1 and our results in Section 4.2.

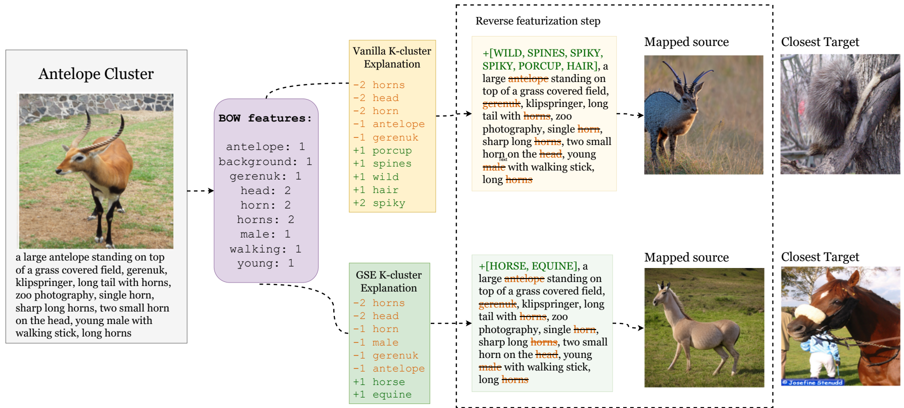

Figure 3: Vanilla vs. GSE K-cluster shift explanations for ImageNet sub-population shifts. Vanilla maps an antelope ("ungulate/hooved mammal" group) cluster shown on the left to porcupines shown on the top right. The explanation of "-2 horns" and "+2 spiky" means that two occurrences of the word "horns" should be removed and "spiky" should be added twice to the caption. In contrast, GSE preserves 'ungulate/hooved mammal' structure, mapping antelope to horses (bottom right). Source images for both techniques are generated using reverse featurization (Section 4).

4.1 Datasets and Experimental Setup

Datasets We perform experiments on tabular, language, and vision data. For tabular data, we use the Adult income (Adult) and Breast Cancer datasets (Breast) [16]. For language data, we evaluate on the Civil Comments dataset [17] (Civil) and Amazon review dataset (Amazon) [18]. Finally, for image data we use the version of the ImageNet dataset from [19] (ImageNet), the FMoW dataset [20], and the iWildCam dataset [21]. Appendix C provides further details on these datasets as well as the source/target splits and group definitions.

Experimental Setup We evaluate three shift explanation methods: K-cluster transport (K-cluster), Optimal transport (OT), and DiCE. Due to space limitations, only the results of K-cluster transport are included in this section and other experiments can be found in Appendix C. For each method, we compare GSE to vanilla explanations. The latter ones are derived by optimizing group-free objectives such as PE in Equation 1 while the former are constructed by optimizing group-aware objectives such as WG-PE in Equation 4.

The three different explanation methods in addition to their counterparts using GSE are evaluated along the following axes: PE and WG-PE where we evaluate over ImageNet pretrained ResNet-50 embeddings for image data; % Feasible from Equation 2; and robustness and worst-case robustness from Equation 3. Further details of the experimental setup are in Appendix D.

4.2 Results

Quantitative results The main quantitative results of vanilla and GSE K-cluster explanations are shown in Table 1-2. We can see from Table 1 that there is often a large gap between the PE and WG-PE, showing the reality of group irregularities across datasets. When comparing GSE explanations to vanilla explanations, GSE almost always results in higher WG-PE (over 20% improvements on the Breast and FMoW datasets) than vanilla explanations, while minimally changing overall PE. Surprisingly, GSE improves PE as seen on the ImageNet, Civil, and iWildCam datasets. GSE also always produces more feasible explanations in comparison to vanilla explanations, and has improvements of up to 22%. This is primarily due to the fact that GSE penalizes explanations with low feasibility. Moreover, according to Table 2, GSE improves both the robustness and worst-case robustness in most cases across all datasets, by as much as 25% (see the Robustness metric for Amazon).

We note that GSE does not result in 100% WG-PE and %Feasible because the K-cluster explanation with 20 clusters is not expressive enough to entirely explain the shift in the distribution. Appendix G has results for more expressive explanation methods.

These results for image data use text-based featurization for interpretability, as discussed in Appendix A.2 and shown in Figure 4. There are other featurization options and Appendix H includes additional results including explanations using raw pixel features. We see the same trends in results for the raw pixel explanations as the text explanations shown here. For full results and comparison with text features, see Appendix H.

Qualitative results A qualitative analysis of GSE explanations for tabular data is given in Figure 1. GSE produces an explanation which modifies age, education level, and occupation instead of changing the infeasible sex attribute like the vanilla explanation. For text data, we analyze an explanation from Civil with respect to its robustness in Figure 2. Finally, for image data, Figure 3 shows a shift explanation for ImageNet where we show the shift in an antelope cluster of the K-cluster explanation. The vanilla explanation maps antelopes to porcupines which breaks the "ungulate/hooved mammal" group, as antelopes are hooved animals while porcupines are rodents. Observing the generated examples for this cluster shows the conversion of an antelope to a porcupine yields unusual-looking results. On the other hand, GSE maps this cluster of antelopes to horses which preserves the groups since horses are also hooved animals. The resulting generated images from this explanation are also clearly images of horses.

5 Related Work

Explaining distribution shift. Kulinski and Inouye [8] proposes three different mappings of varying levels of interpretability and expressiveness as shift explanations. Finding counterfactual explanations to explain model behavior [10] is a related problem, where such explanations represent the minimal perturbation which changes a model's prediction on a given sample [22, 23, 24]. Although not originally created to explain distribution shift, we adapt these methods to our setting (see Appendix A for details).

Worst group robustness. Improving model robustness over sub-populations using group information is extensively studied. Here, the main goal is to minimize the loss on the worst performing sub-population which often becomes a form of distributionally robust optimization (DRO) [25]. The problem of improving model robustness or accuracy on subgroups can be addressed through applications of DRO over subgroups [26, 27], re-weighting sub-populations [28, 29], or performing data augmentation on the worst group [30]. Rather than focus on improving model robustness, our focus is on finding explanations that preserve group structures.

Domain generalization and adaptation. Common solutions for dealing with distribution shift in regards to a model include *domain generalization* and *domain adaptation*. Unlike these methods, our setting is independent of a model. We survey these methods in detail in Appendix I.

6 Conclusion and Future Work

We identified a problem with all existing approaches for explaining distribution shift: the blindness to group structures. Taking group structures into account, we developed a generic framework that unifies existing solutions for explaining distribution shift and allows us to enhance them with group awareness. These improved explanations for distribution shift can preserve group structures, as well as improve feasibility and robustness. We empirically demonstrated these properties through extensive experiments on tabular, language, and image settings.

References

[1] Michael J Kearns and Umesh Vazirani. *An introduction to computational learning theory*. MIT press, 1994.

[2] Alexey Kurakin, Ian J Goodfellow, and Samy Bengio. Adversarial examples in the physical world. In *Artificial intelligence safety and security*, pages 99–112. Chapman and Hall/CRC, 2018.

[3] John R Zech, Marcus A Badgeley, Manway Liu, Anthony B Costa, Joseph J Titano, and Eric Karl Oermann. Variable generalization performance of a deep learning model to detect pneumonia in chest radiographs: a cross-sectional study. *PLoS medicine*, 15(11):e1002683, 2018.

[4] Xiao Wang, Jun Chen, Zheng Wang, Wu Liu, Shin'ichi Satoh, Chao Liang, and Chia-Wen Lin. When pedestrian detection meets nighttime surveillance: A new benchmark. *Image*, 20000(30000):40000, 2020.

[5] Stephan Rabanser, Stephan Günnemann, and Zachary Lipton. Failing loudly: An empirical study of methods for detecting dataset shift. *Advances in Neural Information Processing Systems*, 32, 2019.

[6] Adarsh Subbaswamy and Suchi Saria. From development to deployment: dataset shift, causality, and shift-stable models in health ai. *Biostatistics*, 21(2):345–352, 2020.

[7] manot AI. Why self-driving cars fail: Computer vision challenges for autonomous vehicles, 2022. URL `https://www.manot.ai/why-self-driving-cars-fail-computer-vision-challenges-for-autonomous-vehicles`.

[8] Sean Kulinski and David I Inouye. Towards explaining distribution shifts. In *International Conference on Machine Learning*, pages 17931–17952. PMLR, 2023.

[9] Gabriel Peyré, Marco Cuturi, et al. Computational optimal transport. *Center for Research in Economics and Statistics Working Papers*, (2017-86), 2017.

[10] Ramaravind K Mothilal, Amit Sharma, and Chenhao Tan. Explaining machine learning classifiers through diverse counterfactual explanations. In *Proceedings of the 2020 conference on fairness, accountability, and transparency*, pages 607–617, 2020.

[11] Catherine Blake. Uci repository of machine learning databases. *http://www. ics. uci. edu/˜ mlearn/MLRepository. html*, 1998.

[12] Jean Feydy, Thibault Séjourné, François-Xavier Vialard, Shun-ichi Amari, Alain Trouve, and Gabriel Peyré. Interpolating between optimal transport and mmd using sinkhorn divergences. In *The 22nd International Conference on Artificial Intelligence and Statistics*, pages 2681–2690, 2019.

[13] Rafael Poyiadzi, Kacper Sokol, Raul Santos-Rodriguez, Tijl De Bie, and Peter Flach. Face: feasible and actionable counterfactual explanations. In *Proceedings of the AAAI/ACM Conference on AI, Ethics, and Society*, pages 344–350, 2020.

[14] David Alvarez-Melis and Tommi S Jaakkola. On the robustness of interpretability methods. *arXiv preprint arXiv:1806.08049*, 2018.

[15] Chirag Agarwal, Nari Johnson, Martin Pawelczyk, Satyapriya Krishna, Eshika Saxena, Marinka Zitnik, and Himabindu Lakkaraju. Rethinking stability for attribution-based explanations. *arXiv preprint arXiv:2203.06877*, 2022.

[16] Dheeru Dua and Casey Graff. UCI machine learning repository, 2017. URL `http://archive.ics.uci.edu/ml`.

[17] Daniel Borkan, Lucas Dixon, Jeffrey Sorensen, Nithum Thain, and Lucy Vasserman. Nuanced metrics for measuring unintended bias with real data for text classification. In *Companion proceedings of the 2019 world wide web conference*, pages 491–500, 2019.

[18] Jianmo Ni, Jiacheng Li, and Julian McAuley. Justifying recommendations using distantly-labeled reviews and fine-grained aspects. In *Proceedings of the 2019 Conference on Empirical Methods in Natural Language Processing and the 9th International Joint Conference on Natural Language Processing (EMNLP-IJCNLP)*, 2019.

[19] Shibani Santurkar, Dimitris Tsipras, and Aleksander Madry. Breeds: Benchmarks for subpopulation shift. In *International Conference on Learning Representations*, 2021.

[20] Gordon Christie, Neil Fendley, James Wilson, and Ryan Mukherjee. Functional map of the world. In *Proceedings of the IEEE Conference on Computer Vision and Pattern Recognition*, 2018.

[21] Sara Beery, Arushi Agarwal, Elijah Cole, and Vighnesh Birodkar. The iwildcam 2021 competition dataset. *arXiv preprint arXiv:2105.03494*, 2021.

[22] Sandra Wachter, Brent Mittelstadt, and Chris Russell. Counterfactual explanations without opening the black box: Automated decisions and the gdpr. *Harv. JL & Tech.*, 31:841, 2017.

[23] Chun-Hao Chang, Elliot Creager, Anna Goldenberg, and David Duvenaud. Explaining image classifiers by counterfactual generation. In *International Conference on Learning Representations*.

[24] Shubham Rathi. Generating counterfactual and contrastive explanations using shap. *arXiv preprint arXiv:1906.09293*, 2019.

[25] Aharon Ben-Tal, Dick Den Hertog, Anja De Waegenaere, Bertrand Melenberg, and Gijs Rennen. Robust solutions of optimization problems affected by uncertain probabilities. *Management Science*, 59(2):341–357, 2013.

[26] Shiori Sagawa, Pang Wei Koh, Tatsunori B Hashimoto, and Percy Liang. Distributionally robust neural networks. In *International Conference on Learning Representations*, 2019.

[27] Jingzhao Zhang, Aditya Krishna Menon, Andreas Veit, Srinadh Bhojanapalli, Sanjiv Kumar, and Suvrit Sra. Coping with label shift via distributionally robust optimisation. In *International Conference on Learning Representations*.

[28] Evan Z Liu, Behzad Haghgoo, Annie S Chen, Aditi Raghunathan, Pang Wei Koh, Shiori Sagawa, Percy Liang, and Chelsea Finn. Just train twice: Improving group robustness without training group information. In *International Conference on Machine Learning*, pages 6781–6792. PMLR, 2021.

[29] Jonathon Byrd and Zachary Lipton. What is the effect of importance weighting in deep learning? In *International conference on machine learning*, pages 872–881. PMLR, 2019.

[30] Karan Goel, Albert Gu, Yixuan Li, and Christopher Re. Model patching: Closing the subgroup performance gap with data augmentation. In *International Conference on Learning Representations*.

[31] Clip interrogator. https://github.com/pharmapsychotic/clip-interrogator, 2022.

[32] Robin Rombach, Andreas Blattmann, Dominik Lorenz, Patrick Esser, and Björn Ommer. High-resolution image synthesis with latent diffusion models, 2021.

[33] Pang Wei Koh, Shiori Sagawa, Henrik Marklund, Sang Michael Xie, Marvin Zhang, Akshay Balsubramani, Weihua Hu, Michihiro Yasunaga, Richard Lanas Phillips, Irena Gao, et al. Wilds: A benchmark of in-the-wild distribution shifts. In *International Conference on Machine Learning*, pages 5637–5664. PMLR, 2021.

[34] Sara Beery, Elijah Cole, and Arvi Gjoka. The iwildcam 2020 competition dataset. *arXiv preprint arXiv:2004.10340*, 2020.

[35] Jia Deng, Wei Dong, Richard Socher, Li-Jia Li, Kai Li, and Li Fei-Fei. Imagenet: A large-scale hierarchical image database. In *2009 IEEE conference on computer vision and pattern recognition*, pages 248–255. Ieee, 2009.

[36] Shiori Sagawa*, Pang Wei Koh*, Tatsunori B. Hashimoto, and Percy Liang. Distributionally Robust Neural Networks. In *International Conference on Learning Representations*, April 2020.

[37] Edward J Hu, Phillip Wallis, Zeyuan Allen-Zhu, Yuanzhi Li, Shean Wang, Lu Wang, Weizhu Chen, et al. Lora: Low-rank adaptation of large language models. In *International Conference on Learning Representations*, 2022.

[38] Linoy Tsaban and Apolinário Passos. Ledits: Real image editing with ddpm inversion and semantic guidance. *arXiv preprint arXiv:2307.00522*, 2023.

[39] Been Kim, Martin Wattenberg, Justin Gilmer, Carrie Cai, James Wexler, Fernanda Viegas, et al. Interpretability beyond feature attribution: Quantitative testing with concept activation vectors (tcav). In *International conference on machine learning*, pages 2668–2677. PMLR, 2018.

[40] Alexey Dosovitskiy, Lucas Beyer, Alexander Kolesnikov, Dirk Weissenborn, Xiaohua Zhai, Thomas Unterthiner, Mostafa Dehghani, Matthias Minderer, Georg Heigold, Sylvain Gelly, Jakob Uszkoreit, and Neil Houlsby. An image is worth 16x16 words: Transformers for image recognition at scale. *ICLR*, 2021.

[41] Amirata Ghorbani, James Wexler, James Y Zou, and Been Kim. Towards automatic concept-based explanations. *Advances in neural information processing systems*, 32, 2019.

[42] John X Morris, Volodymyr Kuleshov, Vitaly Shmatikov, and Alexander M Rush. Text embeddings reveal (almost) as much as text. *arXiv preprint arXiv:2310.06816*, 2023.

[43] Adji B Dieng, Francisco JR Ruiz, and David M Blei. Topic modeling in embedding spaces. *Transactions of the Association for Computational Linguistics*, 8:439–453, 2020.

[44] Ryan Greene, Ted Sanders, Lilian Weng, and Arvind Neelakantan, Dec 2022. URL `https://openai.com/blog/new-and-improved-embedding-model`.

[45] Pan Li, Da Li, Wei Li, Shaogang Gong, Yanwei Fu, and Timothy M Hospedales. A simple feature augmentation for domain generalization. In *Proceedings of the IEEE/CVF International Conference on Computer Vision*, pages 8886–8895, 2021.

[46] Huaxiu Yao, Yu Wang, Sai Li, Linjun Zhang, Weixin Liang, James Zou, and Chelsea Finn. Improving out-of-distribution robustness via selective augmentation. In *International Conference on Machine Learning*, pages 25407–25437. PMLR, 2022.

[47] Saeid Motiian, Quinn Jones, Seyed Iranmanesh, and Gianfranco Doretto. Few-shot adversarial domain adaptation. *Advances in neural information processing systems*, 30, 2017.

[48] Shanshan Zhao, Mingming Gong, Tongliang Liu, Huan Fu, and Dacheng Tao. Domain generalization via entropy regularization. *Advances in Neural Information Processing Systems*, 33:16096–16107, 2020.

[49] Yogesh Balaji, Swami Sankaranarayanan, and Rama Chellappa. Metareg: Towards domain generalization using meta-regularization. *Advances in neural information processing systems*, 31, 2018.

[50] Daehee Kim, Youngjun Yoo, Seunghyun Park, Jinkyu Kim, and Jaekoo Lee. Selfreg: Self-supervised contrastive regularization for domain generalization. In *Proceedings of the IEEE/CVF International Conference on Computer Vision*, pages 9619–9628, 2021.

[51] Safa Cicek and Stefano Soatto. Unsupervised domain adaptation via regularized conditional alignment. In *Proceedings of the IEEE/CVF international conference on computer vision*, pages 1416–1425, 2019.

[52] Kuniaki Saito, Yoshitaka Ushiku, Tatsuya Harada, and Kate Saenko. Adversarial dropout regularization. In *International Conference on Learning Representations*.

[53] Da Li, Yongxin Yang, Yi-Zhe Song, and Timothy Hospedales. Learning to generalize: Meta-learning for domain generalization. In *Proceedings of the AAAI conference on artificial intelligence*, volume 32, 2018.

[54] Peter Bandi, Oscar Geessink, Quirine Manson, Marcory Van Dijk, Maschenka Balkenhol, Meyke Hermsen, Babak Ehteshami Bejnordi, Byungjae Lee, Kyunghyun Paeng, Aoxiao Zhong, et al. From detection of individual metastases to classification of lymph node status at the patient level: the camelyon17 challenge. *IEEE transactions on medical imaging*, 38 (2):550–560, 2018.

[55] Soheil Kolouri, Kimia Nadjahi, Umut Simsekli, Roland Badeau, and Gustavo Rohde. Generalized sliced wasserstein distances. *Advances in neural information processing systems*, 32, 2019.

[56] Svetlozar T Rachev and Ludger Rüschendorf. *Mass Transportation Problems: Volume I: Theory*, volume 1. Springer Science & Business Media, 1998.

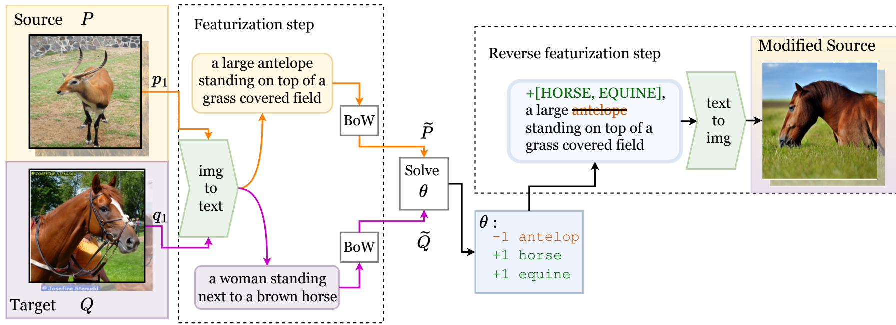

Figure 4: Pipeline of generating a shift explanation for an image. First, each image from the source and the target is transformed to a caption using a pretrained image-to-text model. For each caption, we derive shift explanations over interpretable features, i.e., BoW features (denoted by $\widetilde{P}$ and $\widetilde{Q}$ for source images and target images respectively). The modified caption is then produced from the shift explanation, which is fed to a pretrained text-to-image model for reverse featurization.

A Additional Framework Instantiations

A.1 Generalizing to other shift explanation methods

Generalizing the Mapping $M(x;\theta)$ Recall that shift explanations produced by K-cluster transport can be represented by the mapping function $M(x;\theta)$, which can be any function taking the sample $x \in P$ and the moving distance θ as input. For example, for optimal transport, $M(x;\theta) = x + \theta_x$ where the moving distance, θ_x, varies between different x.

Generalizing the Objective Function beyond PE So far we have only introduced one objective function, PercentExplained (PE), for optimizing the parameters of the mapping function. Indeed, we can replace PE by any differentiable loss function, $L(\theta; M, P, Q)$. For instance, for optimal transport and K-cluster transport, L is $1-$ PE. The details of instantiating M and L for other shift explanation methods, e.g., optimal transport and DiCE, are in Appendix A. Note that the feasibility and robustness metrics introduced in Section 2 (and formalized in Section 3.2) are not suitable due to their non-differentiability. Therefore, they only serve as post-hoc evaluation metrics.

We can now provide a general form of GSE for any shift explanation method decomposed as a parameterized mapping $M(\cdot;\theta)$ and an objective function L for learning θ. First, we extend our formulation of WG-PE in Equation 4 beyond PE by replacing PE with $1-L$ (recall that L is $1-$ PE for K-cluster transport), i.e:

$$\text{WG-}L(\theta; M, P, Q) = \min_g(\{1 - L(\theta; M, P_g, Q_g)\}_{g=1}^{G}) = \max_g(\{L(\theta; M, P_g, Q_g)\}_{g=1}^{G}) \tag{5}$$

Recall that P_g and Q_g represent a group of samples from the source and target respectively, belonging to the same group. We further generalize Equation 5 by using an arbitrary aggregation function F in place of the $\max$ function and regularizing with the loss calculated between the whole P and Q to balance the optimization between the worst group and the overall distribution, i.e.:

$$\text{WG-}L(\theta; M, P, Q) = F(\{L_g(\theta; M, P_g, Q_g)\}_{g=1}^{G}) + \lambda \cdot L(\theta; M, P, Q) \tag{6}$$

where λ is a hyper-parameter and F is an aggregation function. The choice of F and λ for our experiments is given in Appendix D.4.

A.2 Generalizing to language and image data

Since shift explanations are built upon interpretable features, for instance the age and education level for the Adult dataset, we need such interpretable features to produce shift explanations for image and language data. Therefore, we add two additional steps in our framework. The first is a *featurization step*, which extracts interpretable features from the language and image data. Second, we add a *reverse featurization step* for converting modifications to the interpretable features back to the raw data space for producing mapped source samples.

For language data, the featurization step leverages techniques such as Bag-of-words (BoW) and N-Gram models to produce token-level features. Therefore, in the reverse featurization step, we follow the explanations to either remove words or prepend words to the beginning of the input sentences. For image data, the featurization step leverages image-to-text models such as CLIP Interrogator [31] to produce captions for each image from the source distribution and the target distribution. These captions are then processed in the same manner as language data to obtain interpretable features, such as BoW features. Finally, the reverse featurization step follows the explanation to produce modified captions for each source image, which is then transformed back to an image using a text-to-image model such as stable diffusion [32].

A.3 Optimal Transport (OT)

Similar to K-cluster Transport (K-cluster) [8], Optimal Transport (OT) finds the moving distance $\theta(x)$ for shift explanations directly. In the next two sub-sections, we discuss how to instantiate $M(x;\theta)$ and $L(\theta; M, P, Q)$ for OT within our framework.

Mapping function for OT. In OT, the mapping is almost the same as that for K-cluster except that the moving distance θ now depends on each individual sample, x, from the source. Therefore, the counterfactual mapping $M(x;\theta)$ can be written as $M(x_i;\theta_i) = x_i + \theta_i$ for every $x_i \in P$.

Objective function for OT. The objective function for OT is exactly the same as that for K-cluster which is the PE metric. The optimization now results in learning $\theta = \{\theta_1, \ldots, \theta_{|P|}\}$, or a separate moving distance for every source sample such that the PercentExplained is maximized.

A.4 DiCE

For vanilla counterfactual explanation methods such as DiCE, model behavior for a given sample x is explained. To construct such explanations, these methods perform counterfactual modifications to x such that the model prediction changes. We adapt these methods to construct a surrogate shift explanation by finding counterfactual examples for models that classify between source and target distributions. In this subsection, we investigate how general methods for finding counterfactual examples can be adapted to fit within our framework. We take DiCE as an example to describe how to instantiate $M(x;\theta)$ and $L(\theta; M, P, Q)$ for these methods.

Mapping function for DiCE. The counterfactual examples produced by DiCE depend on a given model (parameterized by θ). As a consequence, the mapping function for DiCE, $M(x,\theta)$, is represented as $M(x,\theta) = x + f(x;\theta)$. Let h denote the fixed model which classifies between the source and target data. The moving distance, $f(x;\theta)$, used in the counterfactual explanation relies on this model, h, that DiCE is used to explain.

Objective function for DiCE. As indicated above, it is essential to obtain the parameter θ to learn the shift explanation. Since the model, h, discriminates between the source data, P, and the target data, Q, we optimize the following objective function for DiCE, in which all source samples and target samples are labeled as 0 and 1 respectively:

$$\begin{aligned} &\arg\min_{\theta} L_{\mathsf{DiCE}}(\theta; M, P, Q) \\ &= \arg\min_{\theta} \sum_{x,y \in D} \ell(h(x;\theta), y). \end{aligned} \tag{7}$$

In the above formula, the loss $\ell(\cdot)$ represents the Cross Entropy loss and h denotes the model which classifies between the source and target data $D = \{(x, 0) : x \in P\} \cup \{(x, 1) : x \in Q\}$. Note that the above loss function is an instantiation of the abstract objective function, L, used in Equation equation 6. This optimization leads to learning a θ which is the model parameter for the classifier between the source and target. Once we have learned the model parameter for the model h to be explained with DiCE, we derive the moving distance as

$$\begin{aligned} &f(x;\theta) = \mathsf{argmin}_{\delta_x} \mathsf{dist}(x, x+\delta_x) \\ &\textit{s.t. } h(x+\delta_x;\theta) = 1. \end{aligned} \tag{8}$$

For any $x \in P$ the moving distance $f(x;\theta)$ is found such that it is a minimal change to x which results in the previously learned classifier, h, classifying the modified sample as a target sample.

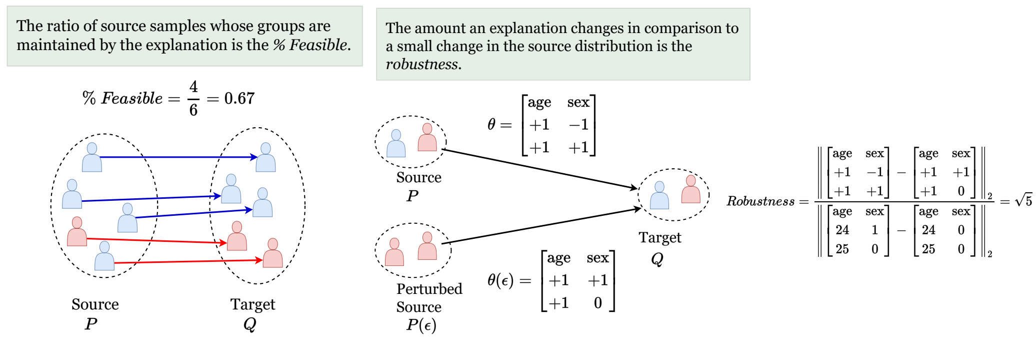

(a) % Feasible (b) Robustness

Figure 5: Visualizations of feasibility and robustness. % Feasible is shown in Figure 5a and it measures the percent of samples which are mapped by $G(x;\theta)$ to a sample with the same group as the original sample. Robustness is shown in Figure 5b and it measures how small perturbations on the source data distribution change shift explanation.

B Details on Feasibility and Robustness

Feasibility and robustness are defined in Equation 2 and 3 respectively, but here we give a visual example of each. A concrete example for calculating feasibility is shown in Figure 5a. The source cluster of four males and one female becomes three males and two females from the mapping, so feasibility is $\frac{4}{6} = 0.667$.

Similarly, we calculate robustness for an example in Figure 5b. Suppose there are two clusters in the source distribution and the target distribution respectively, and each cluster consists of a single sample. After applying K-cluster transport, the moving distance θ from the source to the target can be interpreted as "increasing the age by 1 and flipping the sex attribute". After perturbing the sex attribute of one source sample from 1 to 0, the magnitude of changes on the source data distribution is $\|P - P(\epsilon)\|_2 = 1$. This produces a new moving distance $\theta(\epsilon)$, which is interpreted as "increasing the age by 1 and only flipping the sex attribute of the first source sample". By leveraging Equation equation 3, the Robustness measure Ω for this example is $\frac{\|M(P;\theta)-M(P(\epsilon);\theta(\epsilon))\|_2}{\|P-P(\epsilon)\|_2} \approx \frac{\|\theta-\theta(\epsilon)\|_2}{\|P-P(\epsilon)\|_2} = \sqrt{5}$.

The details for how we produce a perturbation, calculate worst-case robustness, and perform the robustness experiment are given in Appendix D.5.

C Datasets

The tabular, language, and image datasets that we use in the experiments are described in this section.

C.1 Tabular data

Dataset overview. The Adult dataset and the Breast Cancer dataset are standard tabular datasets from the UCI Machine Learning Repository [16]. The Adult dataset consists of 48,842 samples with categorical and integer features from census data. The typical task is to predict whether income exceeds $50K per year. The Breast Cancer dataset contains 569 samples with 10 real-valued features relating to an imaged cell. This dataset is similarly used for binary classification between the classes of benign and malignant tumors.

Distribution shift setup. For both the Adult and Breast Cancer datasets, we match the setup by [8] and consider distribution shift between the different class labels: above 50k and below 50K for Adult, and benign and malignant for Breast Cancer.

Sub-population setup. For the Adult dataset, we use the existing demographic feature of "male" to define two groups. For the Breast Cancer data, we define groups by thresholding on a new attribute which is calculated by using "cell radius" and "cell area" attributes (see Appendix D for details). This leads to 3 groups in total.

C.2 Language data

Dataset overview. The Civil Comments dataset [17] and the Amazon review dataset [18] are used for our language application. The Civil Comments dataset targets predicting the toxicity of up to 2 million public comments and it additionally contains annotations of demographic categories including gender, race, and religion of the authors of each comment. The Amazon review dataset is used for sentiment classification where there is a distribution shift between the subpopulations of reviewers. These datasets are part of the WILDS [33] distribution shift benchmarks and they are used to benchmark subpopulation shift. Subpopulation shift occurs when the proportions of samples from different demographic categories changes between the source and target.

Distribution shift, sub-population and featurization setup. For the Civil Comments dataset, we build a distribution shift setting by splitting it into toxic and non-toxic text as the source and target respectively as done by [8]. After balancing the size of this split, there are 4,437 samples in each of the source and target. The groups are defined by samples with and without the "female" demographic feature. For the Amazon review dataset, we use the default split from the WILDS benchmark which splits the data into two sets of reviews with reviews from different reviewers between the two sets, and we define two groups based on the year the review was written. After balancing the size of the source and target, there are 4,910 samples in each.

The interpretable features for this data are defined by the bag-of-words representation for each sample. We limit the bag-of-words to 50 words which we find helps to avoid model overfitting when using DiCE.

C.3 Image data

Dataset overview. For image data, we use BREEDS [19], FMoW [20], and iWildCam [34]. The BREEDS dataset is a collection of ImageNet [35] subsets created using the wordnet class hierarchy for sub-population shift studies. For our experiments, we take a subset of the ImageNet validation set based on a subpopulation shift between hooved mammals and rodents. The FMoW dataset consists of over 1 million satellite images labelled with one of 62 building or land use categories. This dataset is used to study domain generalization and subpopulation shift since it additionally provides geographic region and time attributes which can be used for creating subsets exhibiting different distribution shifts. Finally, the iWildCam dataset consists of camera trap images taken in different geographic regions. This dataset is used to study subpopulation shift because the distributions of animals shifts between regions.

Distribution shift setup. In BREEDS, We start at the subtree under "mammal" in ImageNet's wordnet hierarchy and select three ImageNet classes under the superclass "rodent/gnawer" and three classes under the superclass "ungulate/hooved mammal" for both the source and target. These three classes for each superclass are chosen in an adversarial way according to [19] to increase the level of subpopulation shift. In total, this subset consists of 298 samples in each of the source and target. In our experiments on FMoW, we subset to the first three land use / building classes and construct the source distribution from samples taken before 2012 and the target from samples taken after 2012 which results in 253 samples for the source and 279 samples for the target. In our experiments on iWildCam, we take the source distribution as images from a single region and the target distribution as images from a separate region. This results in 204 samples for the source and target each.

Featurization and sub-population setup. As described in Section A.2, features for BREEDS and iWildCam are extracted by using an img-to-text model and then treating the caption as a bag-of-words representation. We use a total of 50 words in the bag-of-words as features. Groups are defined for BREEDS by the superclasses "rodent/gnawer" and "ungulate/hooved mammal" to encourage an explanation which does not map rodents to hooved mammals. This grouping allows us to define an infeasible explanation as one which maps rodents to hooved mammals or vice versa. For the FMoW dataset, we featurize based on raw pixel values since the text-to-image model does not perform well on generating satellite images. To construct groups, we use the provided geographic region attribute to define groups since we want our distribution shifts to respect geographic boundaries. For the iWildCam dataset, we define groups by the daytime and nighttime attribute of the images since we don't expect that animals in one region will become nocturnal in another region.

Table 3: Learning rates for all experiments

Dataset	OT	K-cluster	DiCE
Adult	0.1	0.5	0.1
Breast	0.1	5	0.5
Civil	0.1	0.5	0.5
ImageNet	0.5	1.0	0.5
FMoW	0.1	0.5	0.005
iWildCam	1.0	1.0	0.5
Amazon	0.5	0.5	0.5

Note that for datasets such as Civil Comments, iWildCam, and FMoW, the groups are determined by extra annotations which are not available after mapping the source samples by the shift explanations. To determine the group assignments of a mapped source sample, we leverage the group annotation of the mapped sample's closest target sample as an approximated annotation.

D Datasets and Hyperparameters for Experiments

D.1 Tabular data

All categorical features in the Adult data are one-hot encoded resulting in a total of 35 features. We balance the size of both source and target distribution which results in a total of 15,682 samples for the Adult data and 424 samples for the Breast dataset.

The new meta-feature that is used for grouping the Breast dataset is calculated by the expression

$$\frac{\text{Avg. cell radius}^2}{\text{Avg. cell area}},$$

and then we group the data by thresholding on this meta-feature. To find a good threshold, we compute the meta-feature for the entire source and target dataset and get the first and third quartiles. Thus, we create three groups: samples with meta-feature value below the first quartile, between the first and third quartile, or above the third quartile.

When learning vanilla and GSE explanations, we use the same hyperparameters between both. For all methods, we optimize for 200 iterations and list all the specific hyperparameters in Table 3. For DiCE, we use a neural network with a single hidden layer of size 16 as the source vs. target discriminator in all experiments. This network is trained for 500 iterations, with a weight decay of 0.0001. For GSE DiCE, we train the neural network using group DRO [36] with the same hyperparameters used for the vanilla training.

D.2 Language data

For the K-cluster experiments, we use 4 clusters and optimize for 200 iterations using a learning rate of 20. For OT explanations, we optimize for 200 iterations using a learning rate of 0.1. Finally, for the DiCE explanations we first train a logistic regression classifier for classifying the source and target samples using 1000 epochs with learning rate of 0.5 and weight decay of 0.0001. For GSE with DiCE, we train this logistic regression classifier using group DRO with the same hyperparameters used in the regular training procedure.

D.3 Image data

For K-cluster explanations, we use 5 clusters and optimize for 100 iterations using a learning rate of 150.0. For OT explanations, we optimize for 100 iterations using a learning rate of 0.5. Finally, for the DiCE explanations we first train a logistic regression classifier for classifying the source and target samples using 100 epochs with learning rate of 0.1 and weight decay of 0.0001, and we use group DRO to train this classifier for GSE.

D.4 Framework hyperparameters

For all experiments, we use the sum function $F(X) = \sum_{x \in X} x$ for the function F in Equation 6. We also experimented with group DRO loss [36] and $F(X) = \max X$ with $\lambda = 0.1$. Note that for the summation $F(X)$, it is only applicable to the loss function L which does not preserve the addition operation over groups, such as PE. Otherwise, Equation 6 could be rewritten as $\min_\theta ((1+\lambda) \cdot L(\theta; M, P, Q))$, which is not a group-aware loss.

D.5 Robustness experiment

To compute the robustness metric, we use a random small perturbation to the source distribution. To create this perturbation, we randomly select 75% of the features and perturb 1% of the feature values for each of these features. The manner in which we perturb this 1% of the feature values depends on the type of the feature. For real valued features, we find the standard deviation of the feature value for the current feature we are perturbing and we randomly either add or subtract $0.05 \cdot$ stdev to 1% of the feature values. For integer features, we randomly either add or subtract 1 to 1% of the feature values. Finally, for boolean features, we randomly either flip the label of 1% of the True feature values or 1% of the False features values. For categorical features, we first convert the categories to integers such that each category is given an integer from 0 to K-1 where K is the number of categories. This allows us to generate a perturbation for categorical features in the same way as for integer features.

We use the same hyperparameters as above for learning each shift explanation on the perturbed distribution. To speed up the experiments, we first train the shift explanation on the original source distribution and then initialize the parameters of the shift distribution with the parameters learned from the original source distribution when learning the shift explanation for the perturbed distribution.

For computing the robustness metric, we use three random perturbations as described above and average the robustness over the three runs. To compute worst-case robustness, we calculate robustness from 100 random perturbations and take the worst (highest) value of robustness from the 100 trials. Since each calculation of robustness requires learning a shift explanation using the vanilla method and GSE, this experiment is time consuming, so we don't report error bars for the worst-case robustness.

D.6 Compute details

For all experiments, we use a local server with four Nvidia 2080 Ti GPUs and 80 Intel Xeon Gold 6248 CPUs. Each experiment required around 2 GB of GPU memory.

E Experiments Without Group Labels

It is possible that group labels are not always available for a dataset, but we can still use either pretrained models to extract attributes to use for defining groups or use unsupervised methods for grouping the data. We perform an experiment on the language data to show that our group-aware method is still applicable even without group supervision.

To get groups for the language data, we cluster the sentence embeddings of our source and target data. The sentence embeddings are from a state-of-the-art sentence embedding model, `all-mpnet-v2`[2], and we use K-means clustering with 10 clusters to get 10 groups for the source and target. Experimental results are shown in Table 4, and we see the same trends as for the experiments with specified groups. In particular, our group-aware explanation always results in higher worst-group PE and % Feasible than the regular explanation. The most significant improvement in WG-PE is seen for the OT explanation with a change from 63.07% to 93.48%. Interestingly, we also see that our group-aware explanation has slightly improved overall PE over the vanilla DiCE and K-cluster explanations.

[2] `https://huggingface.co/sentence-transformers/all-mpnet-base-v2`

Table 4: Comparison of distribution shift explanation methods on Civil without groups given.

Method	PE	WG-PE	% Feas.	Robustness	WC Robustness
DiCE	1.08 ± 0.1	-5.84 ± 0.5	54.50 ± 0.82	7.82 ± 0.01	7.93
GSE DiCE	**14.32 ± 0.9**	**7.52 ± 0.5**	**56.33 ± 0.85**	**7.71 ± 0.08**	**7.92**
K-cluster	5.19 ± 1.75	2.64 ± 0.34	66.00 ± 0.71	**3.00 ± 0.20**	4.60
GSE K-cluster	**5.72 ± 0.88**	**3.79 ± 0.27**	**67.00 ± 0.41**	3.02 ± 0.05	**3.21**
OT	**99.89 ± 0.00**	63.07 ± 2.97	55.17 ± 4.11	**1.00 ± 0.02**	**1.05**
GSE OT	98.34 ± 0.28	**93.48 ± 0.26**	**84.67 ± 0.24**	1.06 ± 0.03	1.14

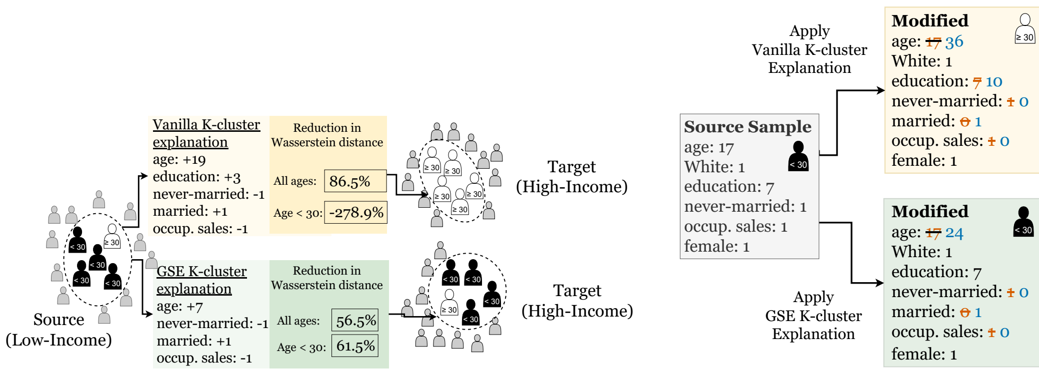

(a) Cluster level shift explanation. (b) Instance level shift explanation.

Figure 6: (a) shows an example shift explanation from a low-income population to a high-income population from the Adult dataset using two different methods: Vanilla K-cluster transport and our GSE K-cluster transport. The shift explanation produced by the Vanilla method explains the shift by increasing age by 19 years, increasing total education by 3 years, making the cluster married, and making the cluster no longer work in sales. On the other hand, GSE generates an explanation that better preserves the subpopulations of people less than 30 and those at least 30 years old depicted as black and white figures respectively, by modifying the age feature by only seven years. The change of $+3$ to education means increasing the maximum education level in grades by three years. (b) shows the instance-level explanation. This explanation changes the sample's age from 17 to 36 whereas our method only increases age to 24.

F Motivating Example Details

F.1 Full Results for Motivating Example

The full results for the explanations shown in the motivating example in Figure 1 and Figure 2.

Table 5: Full results for learning a K-cluster explanation for low to high income shift in the Adult dataset. Groups are defined by Black and White racial groups.

Method	PE	White PE	Black PE	% Feas.	Robustness	WC Rob.
K-cluster	**86.29±0.09**	**87.62±0.06**	51.77±1.60	24.17±2.57	3.69±1.98	6.49
GSE K-cluster	70.22±0.65	68.72±0.80	**67.39±0.05**	**100.00±0.00**	**1.93±0.95**	**3.27**

F.2 Additional Example

We provide another motivating example to show that different choices of infeasible features is possible. Figure 6 can be used in place of Figure 1 and Figure 7a in place of Figure 2a. The choice of which features are infeasible is entirely dependent on the user of the shift explanation and their goals.

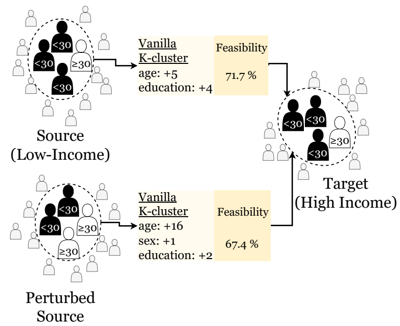

(a) Adult dataset.

Figure 7: Examples of poor robustness of an explanation. Even if an explanation is feasible (top), small perturbations to the source distribution can make it become infeasible (bottom).

G Results for OT and DiCE Shift Explanations

The full results for tabular data, Civil Comments, and ImageNet are given in Table 6, 7, and 8 respectively. With DiCE and OT shift explanations, we see the same trends as previously mentioned in relation to K-cluster explanations. In particular, WG-PE is always improved by GSE, and feasibility and robustness are improved in most cases.

Table 6: Comparison of distribution shift explanation methods on tabular datasets.

Method	PE	WG-PE	% Feas	Robustness	WC Robustness
Vanilla DiCE	2.25 ± 0.29	2.25 ± 0.24	100.0 ± 0.00	23.74 ± 4.05	41.58
GSE DiCE	**26.02 ± 3.00**	**21.69 ± 4.77**	100.0 ± 1.52	**22.34 ± 1.29**	**34.56**
Vanilla OT	95.88±0.08	80.39±0.16	84.87±0.52	**0.77±0.16**	**1.22**
GSE OT	**96.07±0.03**	**90.91±0.17**	**91.7±4.67**	0.79±0.17	1.23

(a) Adult data

Method	PE	WG-PE	% Feas	Robustness	WC Robustness
Vanilla DiCE	29.6 ± 2.43	25.16 ± 1.00	25.94 ± 0.00	**4908.99±3886.07**	15504.20
GSE DiCE	**38.21 ± 1.58**	**33.48 ± 0.40**	**27.20 ± 1.46**	5001.72±2924.73	**11334.15**
Vanilla OT	99.37±0.03	84.10±0.03	39.62±0.77	89.88±24.95	112.00
GSE OT	**99.87±0.00**	**99.37±0.00**	**93.87±0.00**	**45.51±8.20**	**56.44**

(b) Breast data

H Image and Text Featurization Ablation

Table 9 and Table 10 include the results of an ablation on the featurization method used in the experiments. For the BREEDS dataset, we experiment with four different featurization techniques: using raw image pixels, using the Stable Diffusion [32] text-to-image model finetuned on the BREEDS source and target dataset using LoRA [37], using a recent semantic image editing technique LEDITS [38], and using embeddings from a state-of-the-art classification model and interpreting them using concepts [39]. We extract embeddings using ViT-Huge [40] and learn concepts using ACE [41] by constructing roughly 32 patches per image for a sample of 200 images from the source and target and then using KMeans to get 100 clusters in the ViT-Huge embedding space. Once we learn a shift explanation in the ViT-Huge embedding space, we interpret the explanation in terms of the 100 concepts and visualize the explanation for one source cluster in Figure 8.

For the Civil dataset, we experiment with two different featurization techniques: using topic modeling to extract features and perform reverse featurization and using text embeddings from a language model and an embedding inversion technique [42] to interpret them. Specifically, for topic modelling, we follow the topic modeling technique from Dieng et al. [43] to construct a topic model over the Civil source and target data. For the explanation in embedding space, we

Table 7: Comparison of distribution shift explanation methods on language data.

Method	PE	WG-PE	% Feas.	Robustness	WC Robustness
DiCE	2.75 ± 0.19	1.11 ± 0.30	63.33 ± 1.25	5.28 ± 1.72	6.75
GSE DiCE	**19.29 ± 0.80**	**15.12 ± 2.47**	**64.67 ± 0.62**	**1.72 ± 0.06**	**3.40**
OT	3.03± 0.07	2.51±0.16	88.10±0.14	4.45±0.79	5.89
GSE OT	**3.24±0.14**	**3.17±0.12**	**95.07±0.05**	**4.24±0.74**	**5.56**

(a) Civil Comments

Method	PE	WG-PE	% Feas.	Robustness	WC Robustness
DiCE	-17.02±0.19	-17.02±0.19	79.0±0.08	967.04±161.30	–
GSE DiCE	**-16.79±0.18**	**-16.79±0.18**	79.00±0.05	**897.17±127.22**	–
OT	**-1.10±0.02**	**-1.21±0.07**	79.03±0.25	**25.31±5.03**	**36.11**
GSE	-1.25±0.20	-1.25±0.20	**88.10±0.36**	29.60±4.80	36.50

(b) Amazon Review

Table 8: Comparison of distribution shift explanation methods on image data.

Method	PE	WG-PE	% Feas.	Robustness	WC Robustness
DiCE	-1.09 ± 1.54	-17.25 ± 2.55	**50.39 ± 0.42**	**5.08 ± 0.36**	16.24
GSE DiCE	**0.19 ± 1.63**	**-15.27 ± 3.08**	49.94 ± 0.32	6.39 ± 0.64	**15.73**
OT	7.18 ± 1.04	-17.30 ± 2.74	36.12 ± 0.55	18.77 ± 2.56	24.33
GSE OT	**12.81 ± 1.34**	**-14.70 ± 2.50**	**48.16 ± 0.72**	**7.76 ± 1.73**	**22.79**

(a) ImageNet

Method	PE	WG-PE	% Feas.	Robustness	WC Robustness
DiCE	6.26±1.18	-1.02±1.67	67.16±0.40	4.37±0.59	–
GSE DiCE	**7.61±0.22**	**0.92±0.42**	**67.97±0.46**	**3.96±1.01**	–
OT	14.36±0.10	**3.59±0.77**	66.67±0.47	2.89±1.36	7.46
GSE OT	**18.64±0.26**	-1.77±0.58	**100±0.0**	**2.72±1.32**	**7.27**

(b) iWildCam

Method	PE	WG-PE	% Feas.	Robustness	WC Robustness
DiCE	-17.04±0.09	-17.04±0.09	51.52±0.19	**706.15±22.32**	–
GSE DiCE	**-16.57±0.44**	**-16.57±0.44**	**51.65±0.19**	730.96±25.03	–
OT	**98.78±1.42**	-8.34±0.0	47.43±0.0	5.24±0.77	6.82
GSE OT	89.72±0.0	**85.34±0.0**	**97.63±0.0**	**4.75±0.79**	**6.26**

(c) FMoW

use `text-embedding-ada-002` [44] to get text embeddings for all samples in the source and target datasets. After learning a shift explanation, we decode the shifted source centroids to text using vec2text [42]. Figure 9 shows an example explanation learned on text embeddings where we visualize a decoded centroid and the mapped centroid from the Vanilla K-cluster method compared to our K-cluster method.

In general, these results show the same trends as our previous results which empirically supports our claim that our framework is not dependent on a given featurization technique. For BREEDS, even if we choose no featurization (raw pixels), we still see that GSE reduces group irregularities

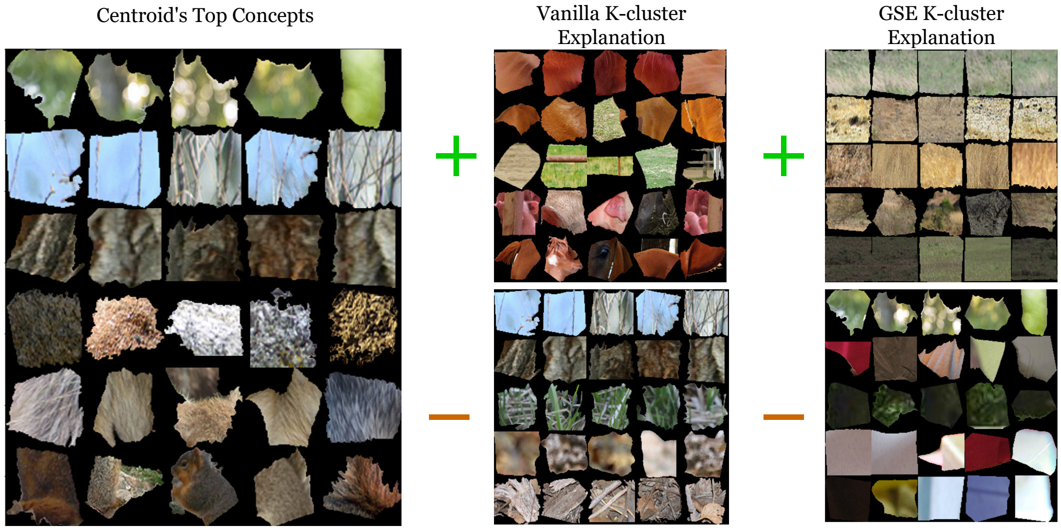

Figure 8: Concept visualization of a Vanilla and GSE K-cluster shift explanation learned for sub-population shift in the BREEDS dataset using embedding space featurization. On the left is are the top concepts for a centroid of the source data where patches from the same concept are in a row and different rows are different concepts. This cluster contains squirrel (rodent), fur, and different tree and grass concepts. The Vanilla explanation adds different concepts associated with pigs and horses (hooved mammals) thus breaking the rodent group of this cluster. The GSE explanation adds different types of grass concepts and removes highly saturated single color concepts and blurred background concepts.

and improves feasibility. Interestingly, there is not always a clear tradeoff between interpretability of the features used and the resulting PE of the explanation. For instance, comparing K-cluster with raw pixel features for BREEDS to K-cluster with text features, we see that pixel features result in slightly lower overall PE than text features. This is because the text-based explanation can add, for example, different horses based on the other features in an image while the pixel explanation must add the same horse to each sample in a cluster.

We emphasize that extracting interpretable features is a separate problem to what this paper studies, but our methods and framework are independent of feature choice, so as new featurization techniques are developed, they can be used with our method.

Some of the worst-case robustness results in Table 9 and Table 10 are marked as "–" since the experiment took too long to run, and we omit DiCE results from the Concepts and Embedding featurization since DiCE did not scale to data with a dimension of 1536 and 768 respectively.

We also visualize the concept featurization explanations and the language embedding featurization explantions. The explanation learned over image embeddings is visualized in Figure 8 in terms of concepts. We learned concepts by taking patches from 200 samples from the source and target and then using KMeans clustering where cluster centroids were treated as concepts. This is equivalent to ACE [41], a common concept extraction method.

I Additional Related Work

Domain generalization and adaptation. Common solutions for dealing with distribution shift include *domain generalization* and *domain adaptation*. Domain generalization assumes that the target distribution is unknown and the goal is to improve model robustness to unseen out-of-distribution data. In contrast, domain adaptation aims to adapt a model learned on the source distributions to some *known target distribution*. But similar techniques were proposed for domain generalization and domain adaptation, including augmenting training data [45, 46, 47], adding regularization terms to the loss function [48, 49, 50, 51, 52] and meta-learning [47, 53]. There are also many real world distribution shift datasets such as the iWildCam dataset [21] and the Camelyon17 dataset of [54] as part of the WILDS datasets [33].

Table 9: BREEDS featurization ablation

(a) Raw pixels

Method	PE	WG-PE	% Feas.	Robustness	WC Robustness
DiCE	-4.22±3.00	-4.87±3.46	54.70±0.55	**1222.97±19.99**	–
GSE DiCE	**-2.32±3.30**	**-2.67±3.79**	**55.26±0.16**	1224.29±51.85	–
OT	100.0±0.0	36.65±0.17	51.45±0.32	581.71±8.97	–
GSE OT	100.0±0.0	**100.0±0.0**	**100.0±0.0**	**1.0±0.0**	–
K-cluster	**13.25±0.05**	9.42±0.06	53.91±0.16	104.59±72.67	–
GSE K-cluster	12.72±0.01	**12.72±0.01**	**57.16±0.32**	**81.56±109.53**	–

(b) Finetuned Stable Diffusion

Method	PE	WG-PE	% Feas.	Robustness	WC Robustness
DiCE	**4.43±0.90**	**-8.58±1.83**	**53.69±1.45**	12.52±3.24	–
GSE DiCE	3.88±1.13	-10.45±2.34	51.57±0.84	**9.96±2.89**	–
OT	18.18±1.19	-9.80±0.63	40.83±0.16	**20.61±6.78**	–
GSE OT	**20.48±0.28**	**-8.24±0.67**	**55.82±1.58**	21.28±7.98	–
K-cluster	7.03±0.57	-14.83±3.01	25.50±2.96	**29.58±1.45**	–
GSE K-cluster	**7.07±0.61**	**-13.09±0.84**	**30.09±1.78**	31.50±2.00	–

(c) LEDITS

Method	PE	WG-PE	% Feas.	Robustness	WC Robustness
DiCE	-0.29±0.14	-7.86±0.54	25.95±0.42	**6.53±0.83**	–
GSE DiCE	**32.32±0.52**	**-2.52±0.70**	**42.51±0.96**	8.33±1.81	–
OT	2.39±0.90	-8.54±0.75	18.57±1.35	**20.61±6.78**	–
GSE OT	**38.58±0.61**	**1.38±0.65**	**47.32±0.27**	21.28±7.98	–
K-cluster	3.74±0.23	**0.48±0.69**	10.62±0.96	**29.58±1.45**	–
GSE K-cluster	**26.92±0.86**	-6.03±0.24	**30.76±1.27**	31.50±2.00	–

(d) Concepts

Method	PE	WG-PE	% Feas.	Robustness	WC Robustness
DiCE	**8.10±0.07**	**3.03±0.08**	76.85±0.47	20.59±3.95	26.08
GSE DiCE	7.65±0.08	2.41±0.03	**77.52±0.47**	**14.32±3.30**	**18.97**
OT	**73.83±0.25**	53.59±0.40	82.77±0.16	35.69±8.93	48.27
GSE OT	71.58±0.25	**67.52±0.05**	**100.00±0.00**	**28.30±2.10**	**31.14**
K-cluster	**28.28±0.48**	16.31±0.09	85.57±0.47	81.42±50.15	151.45
GSE K-cluster	25.93±0.02	**20.75±0.06**	**92.62±0.00**	**37.90±27.15**	**91.64**

J Theoretical Analysis

As mentioned in Theorem 1, to study group irregularities from a theoretical perspective, we consider a simple setting where Wasserstein distance has a closed-form solution. We define our source and target distributions as $P = \text{Bernoulli}(p)$ and $Q = \alpha \cdot \text{Bernoulli}(p) + \beta$ where $p \in [0, 1]$ and $\alpha, \beta \in \mathbb{R}$. In this case, our source distribution consists of a $1 - p$ fraction of the data at $x = 0$ and a p fraction of the data at $x = 1$ while the target consists of a $1 - p$ fraction of the data at $x = \beta$ and the other p fraction of the data at $x = \alpha + \beta$. In this one-dimensional case, we will consider a 1-cluster transport explanation introduced by Kulinski and Inouye [8]. Hence,

Table 10: Civil Comments featurization ablation

(a) Topic Modeling

Method	PE	WG-PE	% Feas.	Robustness	WC Robustness
DiCE	-7.09±0.18	-6.67±0.19	90.56±0.0	**60.54±3.33**	–
GSE DiCE	**-6.50±0.07**	**-6.05±0.12**	**90.89±0.0**	61.64±4.20	–
OT	-10.11±0.31	-10.84±0.46	76.63±0.60	**2.19±0.25**	**2.85**
GSE OT	**-9.85±0.11**	**-9.85±0.11**	**83.23±0.54**	2.31±0.27	3.08
K-cluster	-9.29±0.01	-8.19±0.01	82.53±0.0	4.58±1.92	8.50
GSE K-cluster	**-8.78±0.04**	**-7.65±0.03**	**82.80±0.0**	**2.70±0.84**	**5.19**

(b) Embedding

Method	PE	WG-PE	% Feas.	Robustness	WC Robustness
OT	**81.35±0.21**	19.32±0.13	82.95±0.11	1.28±0.06	1.32
GSE OT	67.42±1.16	**65.19±1.22**	**100.00±0.00**	**1.19±0.05**	**1.25**
K-cluster	**6.18±0.02**	4.04±0.00	82.88±0.16	**0.56±0.02**	**0.57**
GSE K-cluster	5.21±0.71	**4.96±0.88**	**85.15±0.57**	0.65±0.06	0.74

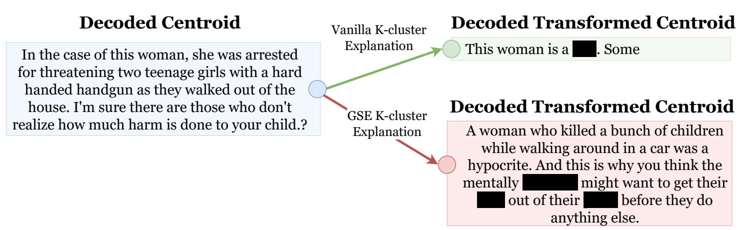

Figure 9: Visualization of a Vanilla and GSE K-cluster shift explanation learned for non-toxic to toxic shift in the Civil dataset using an embedding space featurization. Inappropriate words are redacted. The cluster centroid embedding is decoded to text using the embedding inversion model vec2text. This visualized cluster consists mostly of discussions of crimes and legal cases somehow involving women. The vast majority of the comments in this cluster are written by women but get mapped by the Vanilla explanation to a comment that is far from other comments written by women (it contains a slur for a woman). On the other hand, the GSE explanation makes the source centroid more toxic while making it align better with the group of comments written by women.

given this context, we can first optimize PE(θ) and WG-PE(θ) to obtain the value of θ_{PE} and θ_{WG}, i.e.:

Lemma 2. *Given the context in Theorem 1, maximizing PE(θ) and WG-PE(θ) respectively yields the solution θ_{PE} and θ_{WG} as follows:*

$$\theta_{PE} = (\alpha - 1)p + \beta, \theta_{WG} = \frac{2\beta(\alpha + \beta - 1)}{\alpha + 2\beta - 1} \tag{9}$$

Proof. The overall proof is composed of two steps. The first step explicitly calculates the Wasserstein-2 distance between the source and target distributions, which is followed by the calculation and optimization of PE(θ) and WG-PE(θ) for Vanilla explanations and GSE explanations respectively.

Step 1: calculating Wasserstein-2 distance According to [55], we can obtain the closed-form solution of the Wasserstein-2 distance between two distributions P and Q, i.e.:

$$W_2^2(P, Q) = \int_0^1 \left|F_p^{-1}(u) - F_q^{-1}(u)\right|^2 du, \tag{10}$$

where F_P and F_Q are the Cumulative Distribution Function of the distribution P and Q and thus F_P^{-1} and F_q^{-1} represents the quantile functions of P and Q.

Given that P and Q are Bernoulli distributions, F_P^{-1} and F_q^{-1} are derived as follows:

$$F_p^{-1}(q) = \begin{cases} 0 & q < (1-p) \\ 1 & q \geq (1-p) \end{cases} \qquad\qquad F_q^{-1}(q) = \begin{cases} \beta & q < (1-p) \\ \alpha+\beta & q \geq (1-p) \end{cases}.$$

By plugging the above formula into equation 10, $W_2^2(P,Q)$ becomes:

$$W_2^2(P,Q) = (1-p)\beta^2 + p(1-\alpha-\beta)^2 \tag{11}$$

Similarly, for the mapped source distribution $M(P;\theta) = \{x+\theta; x \in P\}$ after we apply the mapping M, the quantile function of $M(P;\theta)$ becomes:

$$F_{M(P;\theta)}^{-1}(q) = \begin{cases} \theta & q < (1-p) \\ 1+\theta & q \geq (1-p) \end{cases}$$

which is then plugged into equation 10 to calculate the Wasserstein-2 distance between $M(P;\theta)$ and Q:

$$W_2^2(M(P;\theta),Q) = (1-p)(\theta-\beta)^2 + p(1+\theta-(\alpha+\beta))^2 \tag{12}$$

By denoting group 1 and 2 from the source distribution P as P_1 and P_2 and group 1 and 2 from the target distribution Q as Q_1 and Q_2 respectively, we can also calculate the Wasserstein-2 distance within each group in a similar fashion:

$$W_2^2(P_1,Q_1) = |\beta|^2 \tag{13}$$

$$W_2^2(M(P_1;\theta),Q_1) = |\theta-\beta|^2 \tag{14}$$

$$W_2^2(P_2,Q_2) = |1-(\alpha+\beta)|^2 \tag{15}$$

$$W_2^2(M(P_2;\theta),Q_2) = |1+\theta-(\alpha+\beta)|^2 \tag{16}$$

Step 2: calculating and optimizing PE(θ) and WG-PE(θ) By plugging equation 11 and equation 12 to equation 1, we can further calculate PE(θ) as follows:

$$\begin{aligned}\text{PE}(\theta) &= 1 - W_2^2(M(P;\theta),Q)/W_2^2(P,Q) \\ &= 1 - \frac{(1-p)(\theta-\beta)^2 + p(1+\theta-(\alpha+\beta))^2}{(1-p)\beta^2 + p(1-\alpha-\beta)^2}.\end{aligned}$$

Through some algebraic manipulations, we simplify the above formula as follows:

$$\text{PE}(\theta) = 1 - \frac{(\theta - p(\alpha-1)-\beta)^2 + p(1-p)(\alpha-1)^2}{(1-p)\beta^2 + p(1-\alpha-\beta)^2}.$$

Therefore, the above formula is quadratic with respect to θ and we maximize PE(θ) when $\theta_{\text{PE}} := \theta = (\alpha-1)p + \beta$.

Similarly, to derive the GSE explanations, we can plug equation 13 - equation 16 into equation 4 to obtain the worst-group objective WG-PE(θ) as follows:

$$\begin{aligned}\text{WG-PE}(\theta) &= \min\left(1 - \frac{W_2^2(M(S_1;\theta),T1)}{W_2^2(S_1,T_1)}, 1 - \frac{W_2^2(M(S_2;\theta),T2)}{W_2^2(S_2,T_2)}\right) \\ &= \min\left(1 - \frac{(\theta-\beta)^2}{\beta^2}, 1 - \frac{((1+\theta)-(\alpha+\beta))^2}{(1-(\alpha+\beta))^2}\right)\end{aligned}$$

Note that since both $1-\frac{(\theta-\beta)^2}{\beta^2}$ and $1-\frac{((1+\theta)-(\alpha+\beta))^2}{(1-(\alpha+\beta))^2}$ are quadratic to θ, then there are three possible θ_{WG} which maximizes WG-PE(θ), i.e., $\theta=\beta$ which maximizes $1-\frac{(\theta-\beta)^2}{\beta^2}$, $\theta = \alpha+\beta-1$ which maximizes the other term while $\theta = \frac{2\beta(\alpha+\beta-1)}{\alpha+2\beta-1}$ which makes these two terms equal[3]. We discuss these three cases respectively as follows.

[3]Note that $1-\frac{(\theta-\beta)^2}{\beta^2} = 1-\frac{((1+\theta)-(\alpha+\beta))^2}{(1-(\alpha+\beta))^2}$ can also happen when $\theta=0$. But this means that no shifts happen, which is thus ignored

Case 1: $\theta_{\textsf{WG}} = \beta$ This case happens when $1 - \frac{(\theta-\beta)^2}{\beta^2} \leq 1 - \frac{((1+\theta)-(\alpha+\beta))^2}{(1-(\alpha+\beta))^2}$. By plugging $\theta = \beta$ into this inequality, we can get the following constraints on α and β:

$$\frac{((1+\theta)-(\alpha+\beta))^2}{(1-(\alpha+\beta))^2} = \frac{(1-\alpha)^2}{(1-(\alpha+\beta))^2} <= 0,$$

which is only valid when $\alpha = 1$, $\theta = \alpha+\beta-1$ and thus $1 - \frac{(\theta-\beta)^2}{\beta^2} = 1 - \frac{((1+\theta)-(\alpha+\beta))^2}{(1-(\alpha+\beta))^2}$.

Case 2: $\theta_{\textsf{WG}} = \alpha+\beta-1$ This case happens when $1 - \frac{(\theta-\beta)^2}{\beta^2} \geq 1 - \frac{((1+\theta)-(\alpha+\beta))^2}{(1-(\alpha+\beta))^2}$. By plugging $\theta_{\text{WG}} = \alpha+\beta-1$ into this inequality, we get the following constraints on α and β:

$$\frac{(\theta-\beta)^2}{\beta^2} = \frac{(\alpha-1)^2}{\beta^2} \leq 0,$$

which is only valid when $\alpha = 1$, $\theta = \beta$ and thus $1 - \frac{(\theta-\beta)^2}{\beta^2} = 1 - \frac{((1+\theta)-(\alpha+\beta))^2}{(1-(\alpha+\beta))^2}$.

Case 3: $\theta_{\textsf{WG}} = \frac{2\beta(\alpha+\beta-1)}{\alpha+2\beta-1}$ This case happens when $1 - \frac{(\theta-\beta)^2}{\beta^2} = 1 - \frac{((1+\theta)-(\alpha+\beta))^2}{(1-(\alpha+\beta))^2}$ holds. As the analysis of Case 1 and Case 2 suggests, WG-PE(θ) gets maximized when the two terms of WG-PE(θ) are equal. Therefore, Case 1 and Case 2 could be regarded as special cases of Case 3. Therefore, this suggests that the Wasserstein-2 distance within each group gets reduced by the same amount when WG-PE is optimized. But it is worth noting that there are two implicit constraints on α and β, i.e., $\alpha+2\beta \neq 1$ and $\beta(\alpha+\beta-1) \neq 0$.

This thus concludes the proof.

□

Given Lemma 2, we can then show the proof of Theorem 1 as follows.

J.1 Proof of Theorem 1

Proof. First of all, by plugging the values of θ_{WG} and θ_{PE} into PE and WG-PE respectively, we can get the following expressions after some algebraic manipulations:

$$\text{PE}(\theta_{\text{PE}}) = 1 - \frac{W_2^2(M(P;\theta_{\text{PE}}),Q)}{W_2^2(P,Q)} = 1 - \frac{p(1-p)(\alpha-1)^2}{(1-p)\beta^2 + p(\alpha+\beta-1)^2}, \tag{17}$$

$$\text{PE}(\theta_{\text{WG}}) = 1 - \frac{W_2^2(M(P;\theta_{\text{WG}}),Q)}{W_2^2(P,Q)} = 1 - \frac{(\alpha-1)^2}{(\alpha+2\beta-1)^2}, \tag{18}$$

$$\text{WG-PE}(\theta_{\text{PE}}) = \min\left(1 - \frac{p^2(\alpha-1)^2}{\beta^2}, 1 - \frac{(1-p)^2(\alpha-1)^2}{(\alpha+\beta-1)^2}\right), \tag{19}$$

$$\text{WG-PE}(\theta_{\text{WG}}) = 1 - \frac{(\alpha-1)^2}{(\alpha+2\beta-1)^2}. \tag{20}$$

The worst-group PE for GSE, i.e., WG-PE(θ), can be written without a $\min$. Plus, PE(θ_{WG}) − WG-PE(θ_{WG}) = 0, which thus finished the part of the proof for GSE.

The rest of the proof concerns the comparison between PE(θ_{PE}) and WG-PE(θ_{PE}), we will show that θ_{PE} has a discrepancy between the resulting PE and WG-PE in most cases, which we call a *group irregularity*. Since WG-PE(θ_{PE}) involves a minimum of two expressions, $1 - \frac{p^2(\alpha-1)^2}{\beta^2}$ and $1 - \frac{(1-p)^2(\alpha-1)^2}{(\alpha+\beta-1)^2}$, we consider the following three cases: the left expression is less than the right expression, the right expression is less than the left expression, or both expressions are equal.

Case 1 Since the left expression is less than the right expression, we know that

$$\frac{p^2}{(1-p)^2} > \frac{\beta^2}{(\alpha+\beta-1)^2}.$$

So we can get the following through algebraic manipulation,

$$(\alpha+\beta-1)^2 > \frac{\beta^2(1-p)^2}{p^2}.$$

We now lower bound the difference between the overall PE and the worst-group PE:

$$\begin{aligned}\mathsf{PE}(\theta_{\mathsf{PE}}) - \mathsf{WG\text{-}PE}(\theta_{\mathsf{PE}}) &= \left(1 - \frac{p(1-p)(\alpha-1)^2}{(1-p)\beta^2 + p(\alpha+\beta-1)^2}\right) - \left(1 - \frac{p^2(\alpha-1)^2}{\beta^2}\right) \\ &= \frac{p^2(\alpha-1)^2}{\beta^2} - \frac{p(1-p)(\alpha-1)^2}{(1-p)\beta^2 + p(\alpha+\beta-1)^2},\end{aligned}$$

Then by leveraging the fact that $(\alpha+\beta-1)^2 > \frac{\beta^2(1-p)^2}{p^2}$, we can derive the lower bound of the above formula:

$$\begin{aligned}\mathsf{PE}(\theta_{\mathsf{PE}}) - \mathsf{WG\text{-}PE}(\theta_{\mathsf{PE}}) &> \frac{p^2(\alpha-1)^2}{\beta^2} - \frac{p(1-p)(\alpha-1)^2}{(1-p)\beta^2 + p\left(\frac{\beta^2(1-p)^2}{p^2}\right)} \\ = \frac{p^2(\alpha-1)^2}{\beta^2} - \frac{p(1-p)(\alpha-1)^2}{(1-p)\beta^2\left(1+\frac{1-p}{p}\right)} &= \frac{p^2(\alpha-1)^2}{\beta^2} - \frac{p^2(\alpha-1)^2}{\beta^2} = 0\end{aligned}$$

Case 2 Since the right expression is less than the left expression, we know that

$$\frac{p^2}{(1-p)^2} < \frac{\beta^2}{(\alpha+\beta-1)^2}$$

so we can get the following through algebraic manipulation,

$$\beta^2 > \frac{(\alpha+\beta-1)^2 p^2}{(1-p)^2}.$$

We now lower bound the difference between the overall PE and the worst-group PE:

$$\begin{aligned}\mathsf{PE}(\theta_{\mathsf{PE}}) - \mathsf{WG\text{-}PE}(\theta_{\mathsf{PE}}) &= \left(1 - \frac{p(1-p)(\alpha-1)^2}{(1-p)\beta^2 + p(\alpha+\beta-1)^2}\right) - \left(1 - \frac{(1-p)^2(\alpha-1)^2}{(\alpha+\beta-1)^2}\right) \\ &= \frac{(1-p)^2(\alpha-1)^2}{(\alpha+\beta-1)^2} - \frac{p(1-p)(\alpha-1)^2}{(1-p)\beta^2 + p(\alpha+\beta-1)^2}\end{aligned}$$

Then based on the fact that $\beta^2 > \frac{(\alpha+\beta-1)^2 p^2}{(1-p)^2}$, we can derive the lower bound of the above formula as follows:

$$\begin{aligned}\mathsf{PE}(\theta_{\mathsf{PE}}) - \mathsf{WG\text{-}PE}(\theta_{\mathsf{PE}}) &> \frac{(1-p)^2(\alpha-1)^2}{(\alpha+\beta-1)^2} - \frac{p(1-p)(\alpha-1)^2}{(1-p)\left(\frac{(\alpha+\beta-1)^2p^2}{(1-p)^2}\right) + p(\alpha+\beta-1)^2} \\ &= \frac{(1-p)^2(\alpha-1)^2}{(\alpha+\beta-1)^2} - \frac{p(1-p)(\alpha-1)^2}{p(\alpha+\beta-1)^2\left(\frac{p}{1-p}+1\right)} \\ &= \frac{(1-p)^2(\alpha-1)^2}{(\alpha+\beta-1)^2} - \frac{(1-p)^2(\alpha-1)^2}{(\alpha+\beta-1)^2} = 0\end{aligned}$$

Case 3 For the final case where the left and right expression are equal, this means that

$$\frac{p^2}{(1-p)^2} = \frac{\beta^2}{(\alpha+\beta-1)^2}.$$

From the analysis in the two above cases, we can see that we have that $\mathsf{PE}(\theta_{\mathsf{PE}}) - \mathsf{WG\text{-}PE}(\theta_{\mathsf{PE}}) = 0$, so there is no disparity between the overall and worst-group PE. We can solve the equality

$$\frac{p^2}{(1-p)^2} = \frac{\beta^2}{(\alpha+\beta-1)^2}.$$

for p to determine what values of p end up in this case. Solving for p results in $p = \frac{\beta}{\alpha+2\beta-1}$ or $p = \frac{\beta}{1-\alpha}$.

We have now shown that group irregularities exist for all p for cases 1 and 2 and that group irregularities do not exist for case 3 when $p = \frac{\beta}{\alpha+2\beta-1}$ or $p = \frac{\beta}{1-\alpha}$, which thus concludes the proof. $\square$

J.2 Analysis of Robustness and Feasibility

First we analyze robustness in a 1D setting using a 1-cluster transport explanation and then we analyze feasibility in the same setting but with an optimal transport explanation.

Robustness is formally defined in Section 3.2 as

$$\Omega(\theta; M, P, Q, \epsilon) = \|M(P;\theta) - M(P(\epsilon);\theta(\epsilon))\|_2 / \|P - P(\epsilon)\|_2.$$

We analyze the robustness of an explanation which optimizes PE and one which optimizes WG-PE with the following theorem.

Theorem 3. *Given the same setting as that in Theorem 1, the robustness with respect to a small perturbation ϵ to p is $\Omega(\theta_{PE}; M, P, Q, \epsilon) = O(\alpha)$ while $\Omega(\theta_{WG}; M, P, Q, \epsilon) = 0$.*

Proof. We will analyze robustness with respect to a small perturbation ϵ to p, the proportion of samples in each group of the source and target. First, as analyzed in Lemma 2, $\theta_{\mathsf{WG}} = \frac{2\beta(\alpha+\beta-1)}{\alpha+2\beta-1}$ is independent of p. Thus, any change to p will not affect the explanation, so $\Omega(\theta_{\mathsf{WG}}; M, P, Q, \epsilon) = 0$. Next, for the regular explanation, $\theta_{\mathsf{PE}} = (\alpha - 1)p + \beta$. Thus,

$$\begin{aligned}\Omega(\theta; M, P, Q, \epsilon) &= \|(\alpha-1)p + \beta - (\alpha-1)(p+\epsilon) - \beta\|_2 / \|\epsilon\|_2 \\ &= \|(\alpha-1)\epsilon\|_2 / \|\epsilon\|_2 \\ &= \|(\alpha-1)\|_2 = O(\alpha),\end{aligned}$$

which concludes the proof. □

For feasibility, we can perform the analysis in more general settings where the shift explanations are in the form of the optimal transport map. An optimal transport explanation has the form $M(x;\theta) = x + \theta(x)$. Based on the solution to the optimal transport problem in 1D [56], the form of the optimal transport map is:

$$\theta(x) = (F_S)^{-1} \circ F_T(x)$$

where F_S is the cumulative distribution function (cdf) of the source, F_T is the cdf of the target. Thus $(F_S)^{-1}$ is the quantile function of the source distribution. When the source and target are defined as Bernoulli distributions, we have the next lemma.

Lemma 4. *Let $\alpha, \beta \in \mathbb{R}$, $p \in [0,1]$, and define $P = \alpha \cdot$ Bernoulli$(p) + \beta$. Then the cdf and quantile functions for P are the following:*

$$F_P(x) = \begin{cases} 1-p & \text{if } x = \beta \\ 1 & \text{if } x = \alpha + \beta \end{cases} \qquad F_P(x)^{-1} = \begin{cases} \beta & \text{if } x \le (1-p) \\ \alpha+\beta & \text{if } x > (1-p) \end{cases}.$$

To analyze feasibility, we use the definition of feasibility from equation 2:

$$\%\ \text{Feasible} = \left[\sum\nolimits_{x\in P} a(x, M(x;\theta))\right] / \|P\|$$

Let $p \in [0,1]$, $\alpha, \beta \in \mathbb{R}$ and define $P =$ Bernoulli(p) and $Q = \alpha \cdot$ Bernoulli$(p) + \beta$. Define groups for $x \sim P$ as group 1 if $x = 0$ and group 2 if $x = 1$. Define groups for $x \sim Q$ as group 2 if $x = \alpha + \beta$ and group 1 if $x = \beta$.

We can write the optimal transport explanation to explain the shift between S and T using Lemma 4 as:

$$M(x;\theta_{\mathsf{PE}}) = \begin{cases} x + \beta & \text{if } x = 0 \\ x + \alpha + \beta - 1 & \text{if } x = 1. \end{cases}$$

We then find the worst-group optimal transport solution. The worst-group optimal transport is an optimal transport in the worst case over the groups of the source and target data. Thus, we have that this worst-case optimal transport has the following form based on the definition of an optimal transport map [56]:

$$\pi^* = \inf_{\pi} \max\left(\int_{x=0,y=\alpha+\beta} \|x-y\|_2^2 d\pi(x,y), \int_{x=1,y=\beta} \|x-y\|_2^2 d\pi(x,y)\right)$$

where π is a valid transport map. Since the subgroups are point distributions, the optimal transport between the two point groups has a direct solution which is to map the source point to the target point. Thus, the worst-group optimal transport is optimal for both groups as seen by the optimal transport explanation shown below:

$$M(x;\theta_{\text{WG}}) = \pi^* = \begin{cases} x+\alpha+\beta & \text{if } x = 0 \\ x+\beta-1 & \text{if } x = 1. \end{cases}$$

Theorem 5. *Let $p \in [0,1]$, $\alpha, \beta \in \mathbb{R}$ and define $P = \text{Bernoulli}(p)$ and $Q = \alpha \cdot \text{Bernoulli}(p) + \beta$. Define groups for $x \sim P$ as group 1 if $x = 0$ and group 2 if $x = 1$. Define groups for $x \sim Q$ as group 2 if $x = \alpha + \beta$ and group 1 if $x = \beta$. Let $M(x;\theta_{PE})$ be an optimal transport explanation and $M(x;\theta_{WG})$ be a worst-group optimal transport explanation. Then, $M(x;\theta_{PE})$ has feasibility of 0 while $M(x;\theta_{WG})$ has feasibility of 1.*

Proof. In the definition of Feasible, we define

$$a(x,y) = \begin{cases} 1 & \text{if } x = 0 \text{ and } y = \alpha+\beta \text{ or } x = 1 \text{ and } y = \beta \\ 0 & \text{otherwise.} \end{cases}$$

This definition encapsulates the desire to keep samples from group 1 in the source in group 1 in the target and the same for group 2. We can immediately see that X_{PE} maps all samples from group 1 in the source to group 2 in the target, so feasibility will be 0. On the other hand, X_{WG} maps samples respecting the defined group structure, so feasibility is 1. □

K Limitations and Societal Impacts

GSE explanations are only as good as the underlying shift explanation method. For instance, K-cluster transport can result in weak explanations that minimally reduce the Wasserstein distance between the source and target distributions if too few clusters are used (i.e. K is chosen too small). On the other hand, the Optimal Transport explanation that we found reduced the Wasserstein distance the most, is not very interpretable since each source sample can be mapped differently. This results in the explanation being interpretable only on a per-sample basis. Improved interpretability of shift explanations is an area for future work.

In addition to interpretability of the explanation, our shift explanations for image and language data rely on interpretable feature extraction methods and methods for counterfactual modification based on changes to the features as described in Section A.2. We designed a system for interpretable feature extraction which uses a bag-of-words feature representation, but this method looses the context that words are used in and it is difficult to make counterfactual modifications. Creating disentangled embedding spaces for interpretable embeddings that can also be used for counterfactual modification is an area of active research, but there is still work left to make these approaches more general.

We also found that GSE is sensitive to the choice of groups. Even though unsupervised methods can be used to select groups as shown in Appendix E, future work can look at how to best select or design groups. For instance, it may be the case that we know of some groups, but we want the rest of the data to be grouped appropriately.

Finally, while we evaluated the worst-case robustness, our method sometimes results in worse worst-case robustness than the vanilla approach. This is again due to the choice of groups. Future work should investigate how to extend group robustness to worst-case group robustness of shift explanations so that a bad choice of groups does not negatively impact robustness.

Explanations which look plausible but are actually wrong can be harmful. This creates the illusion of understanding, and this can have serious downstream implications especially if policies are constructed from a shift explanation. With this work we hope to uncover some properties that a good shift explanation should have and design metrics and learning procedures based on group robustness to rectify these issues.